ELSEVIER

Journal of Volcanology and Geothermal Research 74 (1996) 131–153

Journal of volcanology and geothermal research

Scaling effects on vesicle shape, size and heterogeneity of lavas from Mount Etna

H. Gaonac'h [a,*], J. Stix [a], S. Lovejoy [b]

[a] *Département de Géologie, Université de Montréal, case postale 6128, succursale centre-ville, Montréal, Qué. H3C 3J7, Canada*
[b] *Department of Physics, McGill University, Montréal, Qué. H3A 2T8, Canada*

Received 1 May 1995; revised 1 April 1996

Abstract

The rheology of basaltic lava flows depends on several factors including the vesicle size and shape distributions. We analysed vesicles in lavas from Mount Etna by sawing, painting and digitizing the collected samples. We find statistical properties which are common from one sample to another and which are independent of size for different types of lava including pahoehoe, aa and massive. For example, lava vesicularity shows scale invariant behaviour from ≈ 0.10 to ≈ 4.00 mm implying a simple relationship between vesicularity and the resolution at which it is estimated. In order to deduce the volume distribution from the observed area distribution, we develop transformation rules which apply to vesicles of arbitrary shape. On the 22 out of 25 samples, we find that the vesicle number–size density is scale invariant over the same ranges ($n(V) \propto V^{-B-1}$) with a power law distribution of exponent $B \approx 1$. When averaging over all the samples, the results yield a somewhat more precise estimate $B \approx 0.85$. For small vesicle sizes (typically less than ≈ 0.25 mm^2), another power law with an exponent $B \approx 0$ is found in nearly all samples. Hence, the observed similar scaling behaviours found in the samples reveal the existence of a common vesicle pattern which may be related to vesicle growth mechanisms in very different looking samples. Moreover, even for identical volcanological/geological conditions—when $B \leq 1$—the vesicularity will vary significantly from one sample to another depending on the presence or absence of a few very large vesicles, implying significant spatial rheological variations of the lava flows.

Keywords: lava vesicularity; gas vesicles; scaling; fractal; heterogeneity; Mount Etna; volcanology

1. Introduction

Vesicle size distributions observed in volcanic products characterize the whole vesicle population and provide basic information about vesicle growth mechanisms. The size of gas vesicles can vary from a few microns at the nucleation level to several meters when they burst at the surface of the volcano. In spite of their undoubted importance for understanding both the morphology and rheology of lava flows as well as the associated flow emplacement, to date comparatively little quantitative work has been done. For example, although the effect of various factors on lava rheology, such as the initial temperature, crystallization, eruption rate (see Chester et al., 1985, for a review) has received some attention, little is yet known about the effects of the distribution of sizes and shapes of gas filled vesicles. It is, however, known that changes in overall vesicle content and

* Corresponding author. Fax: (514) 343-5782. E-mail: gaonach@ere.umontreal.ca.

PII S0377-0273(96)00045-5

deformation strongly affect the lava rheology, particularly the relative viscosity, compressibility, cooling and differential internal shearing of the flow (e.g., Jaupart and Vergniolle, 1988; Jaupart, 1991; Stein and Spera, 1992; Bagdassarov and Dingwell, 1993; Wilmoth and Walker, 1993, Keszthelyi, 1994). These studies clearly point to a nonlinear rheological relation between the lava flows and the variability of the vesicle population.

Ratios of a million or more between largest and smallest vesicle volumes are commonly observed even in samples only centimeters across. This in itself makes it unlikely that the basic vesicle growth mechanisms involve a well defined characteristic length. At the same time, it poses problems in the use of standard statistical techniques which are based on the notion of characteristic (e.g., mean or median) vesicle sizes (e.g., Walker, 1989). Such reductions of number distributions to single size values are only justified if the distribution decays rapidly (at least exponentially fast), necessarily involving only narrow ranges of volumes. The limitations of this approach are illustrated by the studies of Sarda and Graham (1990), Mangan et al. (1993) and Cashman et al. (1994) who suggest that vesicle (and crystal) sizes follow exponential distributions while admitting that the major contribution to overall vesicularity is associated with large "outlier" (nonexponential) vesicles. Another limitation of existing studies is that they have been conducted on lavas with spherical (or "near" spherical) vesicles (Walker, 1989; Mangan et al., 1993; Cashman et al., 1994); these are not representative of typical lava. Below we propose methods of overcoming both of these problems.

Rather than attempting to fit distribution data to ad hoc functional forms it would clearly be more profitable to consider the implications of vesicle growth processes on the distributions and derive the latter from theoretical considerations. With this in mind, we quickly survey the various growth processes which have been proposed to explain the observed final vesicle sizes. Starting with nucleation [which may be effective at different times during the ascent, e.g., in the magma chamber, conduits (Vergniolle and Jaupart, 1986), but also in subsurface flows (Cashman et al., 1994)], growth by diffusion and expansion are generally considered as major processes for small to medium vesicles ascending from depth to the surface of the volcano (e.g., Sparks, 1978; Aubele et al., 1988). Toramaru (1990) morphologically analysed vesicles after making "corrections" for their non-spherical shapes and proposed a mean vesicle radius based growth model involving temporal scaling laws (proportional to t^n; t is the time, n an exponent). On the other hand, in studies of high pressure lavas (Sarda and Graham, 1990) and in studies of sub-surface lavas (Mangan et al., 1993; Cashman et al., 1994) it has been suggested—in analogy with crystal size distributions—that vesicle size distributions are exponential. These authors hypothesized that this was the result of continuous and simultaneous nucleation and diffusive growth process and explained departures from exponential distributions as the results of secondary mechanisms such as vesicle coalescence, breakage, ripening. They concluded that coalescence (which—according to Cashman et al., 1994—leads to "perturbations" from exponential distribution) is not important because it does not affect a large number of vesicles.

In contrast, other authors (e.g., Sahagian, 1985; Sahagian et al., 1989; McMillan et al., 1989; Carbone, 1993, Gaonac'h et al., 1996) have suggested that coalescence is an important growth mechanism. Coalescence may be (1) dynamic—via the stochastic collection of neighbouring vesicles moving at various velocities (Gaonac'h et al., 1996)—or (2) static —as triggered by the appearance of diktytaxitic voids, which destroy the walls of adjacent vesicles (Walker, 1989). The vesicle population may also be affected during an eruption by the elimination of vesicles through degassing (Blackburn et al., 1976; Cashman et al., 1994) or by bursting of lava or shearing of vesicles (Walker, 1989). Hence—although there is not as yet any consensus on the importance of the different growth processes at subsurface conditions—none of the proposed mechanisms operates at a well defined characteristic size, but rather over a wide range of sizes, they are "scaling".

In the present paper we argue that this scaling is a fundamental symmetry principle respected by the relevant nonlinear dynamics, and that this provides a unified framework for both analysing and modelling vesicle distributions. Scaling behaviour is indeed ubiquitous in geophysics; it is associated with fractal structures, multifractal statistics and power law dis-

tributions. Directly relevant examples of scaling dynamical processes are the diffusive vesicle growth laws (Sparks, 1978; Toramaru, 1990), and coalescence processes (see Gaonac'h et al., 1996, for a scaling model). For vesicles in a lava sample, scaling means that a function such as the number distribution can be described as a power law: below we confirm this prediction on vesicle distributions from lavas of the 1985 and 1991–1993 Etna eruptions.

The finding that vesicle distributions can be scaling up to the largest vesicle volumes, combined with the importance of vesicles for the rheology of lava (both fluid and solid, e.g., viscosity and yield stress) suggests that the range of vesicle scaling (which a priori is itself highly variable) may be a fundamental determinant of rheological properties. This provides us with a quantitative way of distinguishing the rheology and morphology of lava flows (aspects which are not otherwise easy to disentangle). To illustrate this, consider the morphology of lava flow fields which show great variations of sizes, shapes, and surface textures such as pahoehoe and aa. In spite of these differences, qualitatively similar heterogeneous structures can be found over a large range of scale suggesting similar mechanisms acting at widely varying scales. Gaonac'h et al. (1992) have shown that the lava flow morphologies of different volcanoes have common scaling properties down to at least 10 m. The scale invariance was quantified by exponents (fractal dimensions) relating morphological parameters such as the area or the perimeter of flow fields to the resolution. The knowledge of the inner scale (the small scale where this behaviour breaks down) is then fundamental in estimating true areas and perimeters (as well as other parameters such as eruption rates). On the basis of in situ morphology and texture, it was speculated that this inner scale was less than several meters in size. Independently, Bruno et al. (1992) have found direct evidence that lava flows are indeed scale invariant down to 0.5 m or less.

Different physical effects—acting at different scales—are involved to produce the final flow field pattern, including the topography of the volcano, the rheology of the lava. We speculated that, over a wide range of scales, the observed scale invariance of the morphology may be explained by the scale invariance of the topography (see discussion in Gaonac'h et al., 1992). It is therefore quite possible that the inner scale of the lava flow morphological variability is determined by the outer scale (largest scale of variability) of rheological characteristics (e.g., corresponding to the largest vesicles). In other words, the inner scale of the morphology of flow fields may be explained by a change in the dominant physical process (e.g., rheology becoming more important than topography or other morphologically significant factors).

In this paper we focus on the scaling properties of the heterogeneous distribution of gas vesicles present in basaltic lava, and the consequences especially on the large observed variability in the vesicularity of the lava and hence in its rheology. Aside from this scaling framework, we develop two related methodological innovations which allow us to relatively easily study large numbers of samples. The first is the technique of sawing, painting and digitizing the vesicle pattern. The second is a method of obtaining volume distributions from the available area distributions, using only scaling properties without any assumptions about the shape of individual vesicles (the method is actually more general allowing us to deduce the three-dimensional distributions from observations over any lower dimensional subsets; the details are in Appendix A). In Section 2, we discuss the geology of the sample site (Mt. Etna) and in Section 3, the implications of scale invariance for the distribution functions (the technical details are in Appendix B): we show that the vesicle population can be statistically divided into two regimes characterized by two different exponents. The same exponents are found in virtually all samples, suggesting they each correspond to a basic growth process, identified here with diffusion and coalescence dominated dynamics (small- and large-scale regimes, respectively). While small vesicles are indeed far more numerous it is rather the large vesicles (in many cases the single largest one) which gives the main contribution to the vesicularity. This quantitatively resolves the debate about whether diffusion or coalescence is "dominant"; the former gives the largest contribution to the total number of vesicles, while the latter to the total vesicularity. In Section 4, we consider the problem of estimating the vesicle sizes as a function of the resolution of our measurements, and in Section 5 we sketch some conclusions.

2. Data collection and vesicularity analysis

2.1. Data collection and methodology

Mount Etna has continuous degassing from its summit craters, and erupts hawaiitic lavas every few years. Samples from the 1985 eruption were collected at its initial source at 2590 m above sea level (a.s.l.) (emplaced 12 March 1985), and compared with samples from an ephemeral bocca at 2120 m and an overflow at 2100 m (Fig. 1, sites 1–3; see Gaonac'h, 1994, for more details). The flows from the ephemeral bocca at 2120 m a.s.l. and from the overflow at 2100 m a.s.l. were selected because we had good control on their areal extent (to within a few hundred meters) and because of their relatively small thicknesses (1–2 m), hence avoiding the overlap of flows. We also collected samples at a vertical section (2300 m a.s.l.) of a flow several meters thick to study the vertical vesicle distribution and to compare with our horizontal sampling (Fig. 1, site 4). We collected pahoehoe and aa lava types at each site.

Samples from the 1991–1993 eruption (Barbieri et al., 1993) were also collected (Fig. 1, sites 5 and 6). The samples are from one of the first lava flows on 14–15 December 1991 (2900 m a.s.l.) and from a bocca (collected on 12 January 1992) located at 1200 m a.s.l. and active during January 1992. The latter samples were collected while still incandescent and cooled in the snow. We therefore had good control on the temporal sequence of the samples.

All samples were sawed in half. Their surfaces were painted to enhance the contrast between voids corresponding to vesicles and solid surface, and then digitized, at a resolution of 0.085 mm, with a commercial scanner using 512 × 512 pixels for the larger samples and 512 × 256 pixels for the smaller samples. Two samples (46a, 33a) were sawn twice to expose two mutually perpendicular surfaces. Thin

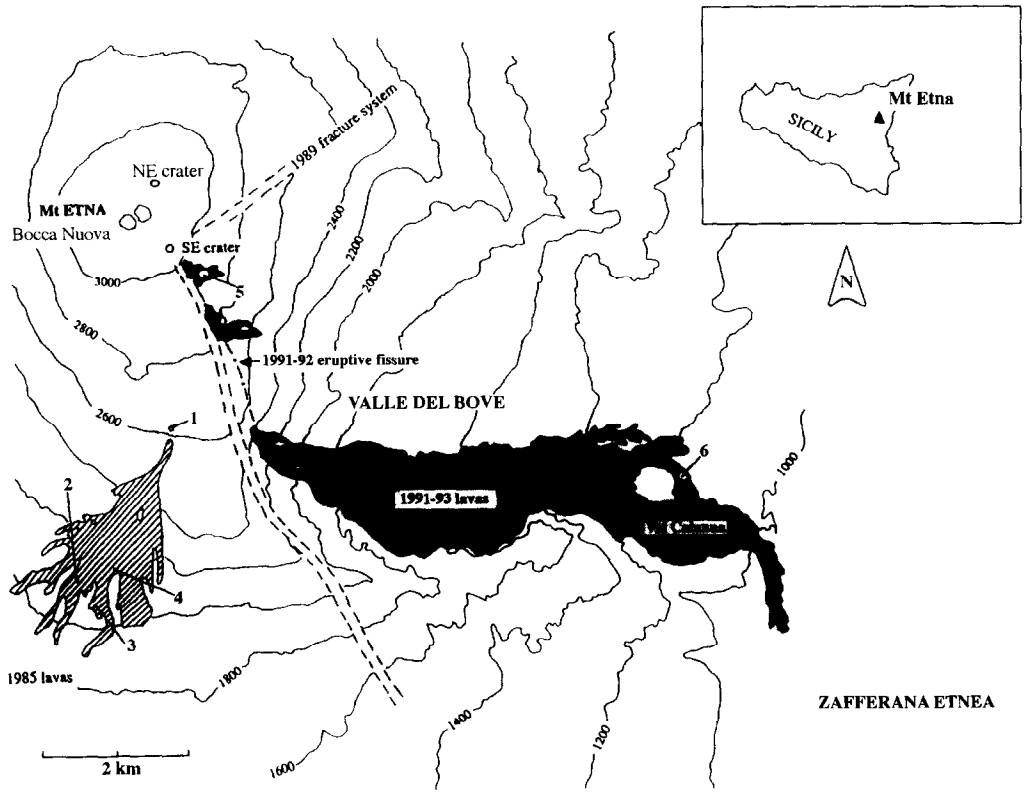

Fig. 1. Map of the 1985 and 1991–93 flow fields from Mount Etna. *1* = 1985 initial source; *2* = 1985 ephemeral bocca; *3* = 1985 overflow; *4* = 1985 vertical section; *5* = 14–15/12/91 (1991–1993 series); *6* = 12/01/92 (1991–1993 series).

sections were made of each sample to qualitatively examine the smallest detectable vesicle size and the relationship between vesicles and crystals. Small blocks measuring $1.5 \times 1.5 \times 3.0$ cm^3 were sawn to estimate the three-dimensional vesicularity (Gaonac'h, 1994).

We observed that the largest size of the vesicles is a function of the size of the sample; for example, we found vesicles of cm order in the cm-sized large sawn samples, whereas they are of mm order in thin sections of the same samples. Vesicles as large as 8–10 cm were observed in the field. As mentioned by Blackburn et al. (1976), and Vergniolle and Jaupart (1986), we expect much larger vesicles to exist in the field that are not preserved in collected samples. A detailed description of the samples used here can be found in Gaonac'h (1994). Fig. 2 and Fig. 3 illustrate the complexity and the variation of the typical vesicle spatial distributions.

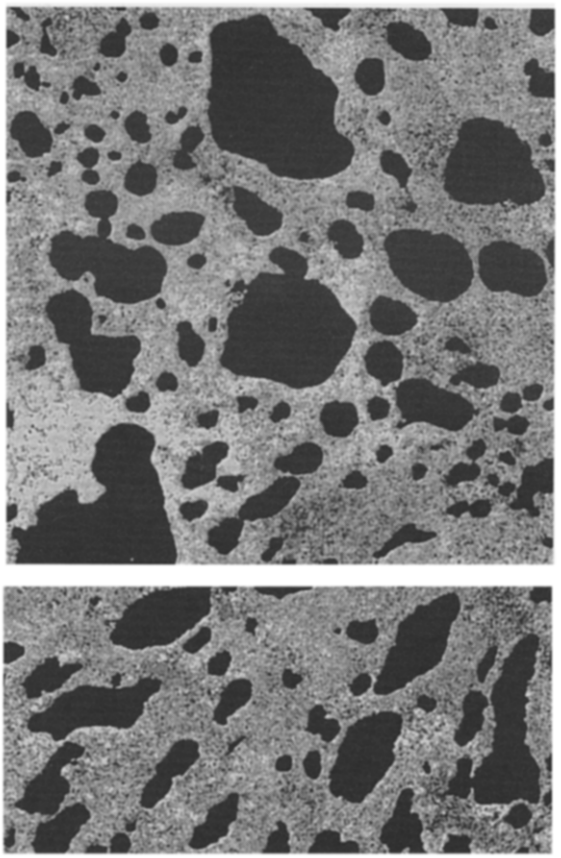

Fig. 2. Digitized orthogonal surfaces from sample 46a collected at 20 cm in depth from the initial 1985 bocca.

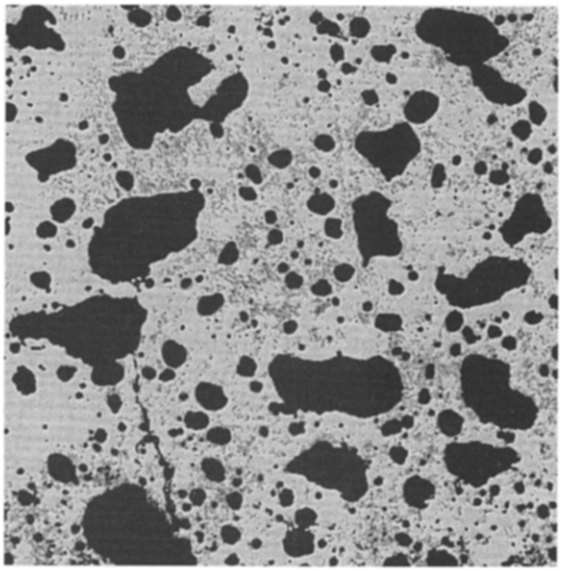

Fig. 3. Digitized surface of sample 32a collected 40 m away from the source of the 1985 overflow.

2.2. Vesicularity

Vesicle anisotropy, deformation, and heterogeneity may affect vesicularity estimates. Fig. 2 is an example of a sample which shows strongly deformed vesicles on one sawn surface and relatively non-deformed vesicles on its perpendicular surface. Anisotropy can systematically bias results if "special" planes (e.g., oriented parallel or perpendicularly to a characteristic direction) are sampled from the rock whereas the heterogeneity/variability can lead to large sample to sample variations (even from neighbouring lavas), particularly since we find that the sample vesicularity can be dominated by a single large vesicle. The large sample variability even leads to difficulties in estimating the 3-D vesicularity from 2-D cross sections. However, when comparing two-dimensional (P_2) and three-dimensional (P_3) vesicularities (Gaonac'h, 1994), the two were generally within one standard deviation error bars (except for samples 46a and 46b). The scaling approach developed in Section 3 enables us to partially overcome this problem by expressing the sample vesicularity as

the product of two factors one dependent on the largest vesicle present and the other on the history/volcanology of the sample.

Two observations may be reported concerning the variation of the vesicularity along flows (Table 1): (1) the highest P_2 values are found at the earlier initial bocca (> 30%) and are probably due to a gas-rich magma that can be correlated with the lack of hornitos and spatter cones in the early stages of the 1985 eruption. The strong, quick and heterogeneous degassing at the initial source can be observed by the large range of vesicularity (25–42%). Samples collected away from the early initial source, with lower P_2 values, were likely derived from lava that had been degassed at the active boccas through hornitos and spatter cones at 2500 m; (2) when plotting the vesicularity of pahoehoe and aa samples (Fig. 4a), we cannot discriminate in a simple manner between the two types according to their vesicularity. The toothpaste lava (17.1%) lies within the pahoehoe and aa ranges. We then turn to the vesicle population itself observed in different types of lava.

3. Number distribution functions

3.1. Power law distributions

Power law distributions occur in many fields of geophysics because they maintain their functional

Table 1
Lava sample, eruption dates and observed two-dimensional vesicularities

Lava type	Sample numbers	Eruption dates	P_2, 2-D vesicularity (%)
Hawaii			
Spongy pahoehoe			50.7
Etna, initial source			
Pahoehoe, surface, Etna	46b	1985	24.8
Aa, initial bocca	46c	1985	35.0
Pahoehoe, 20 cm depth	46a	1985	33.4
Bulb of lava	45	1985	41.5
Etna, overflow			
Massive lava, channel	33c	1985	3.8
Pahoehoe, source of overflow	33a	1985	27.5
Aa, source of overflow	33b	1985	17.2
Pahoehoe, 40 m from the overflow	32a	1985	29.9
Aa, 40 m from the overflow	32b	1985	16.2
Irregular aa, front of the overflow	34a	1985	19.1
Rounded aa, front of the overflow	34b	1985	17.5
Etna, Bocca			
Pahoehoe	22a	1985	19.7
Massive lava, 40 m from the bocca	22c	1985	5.2
Aa, end of flow, 100 m from the bocca	23i	1985	16.3
Etna, vertical section			
Upper aa, Etna	58d	1985	22.8
Massive flow, upper part, Etna	58c	1985	12.6
Massive flow, lower part, Etna	58b	1985	6.3
Basal aa, Etna	58a	1985	16.9
Etna, 1991–1993 series			
Pahoehoe, Etna	07a	14/12/1991	19.3
Aa, Etna, 200 m from bocca	01b	01/1992	15.7
Toothpaste, Etna, bocca	02b	01/1992	17.1
Eroded aa, Etna	01c	01/1992	13.7

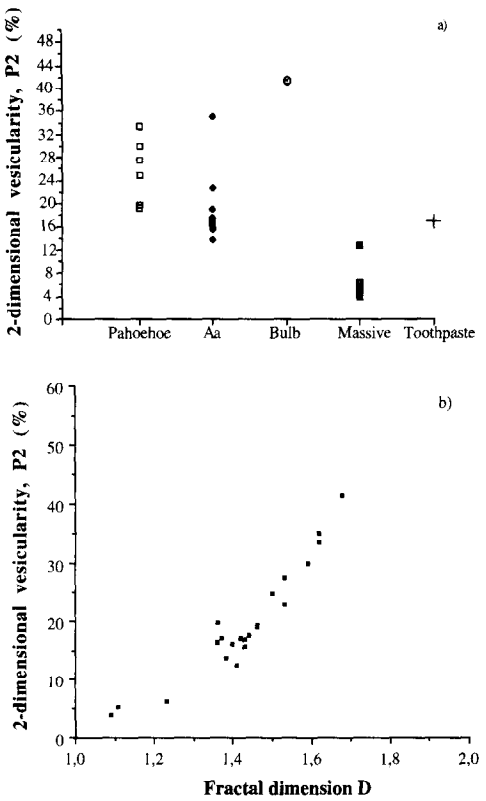

Fig. 4. (a) Vesicularity of 1985 and 1991–1993 samples. (b) Diagrams of 2-D vesicularity, estimated at 300 dots per inch, versus fractal dimension D.

form under changes in scale. Several qualitatively distinct types of power laws have been found to be geophysically relevant. Here we are primarily interested in number size distributions of various sets; if the distribution is scaling then:

$$n(V) \propto \left(\frac{V}{V^*}\right)^{-B-1} \quad (1)$$

where n is the number density [1], V the vesicle volume and V^* a characteristic volume (dependent on lava history/volcanology) discussed below; $\propto$ means "proportionality"; for technical reasons discussed in the appendices, such densities can generally be valid only over finite ranges of V. Geophysically relevant examples of this type of density (with areas rather than volumes) include ocean islands (Korchak, 1938) (it is presumably a consequence of the multifractality/resolution independence of the topography; Lavallée et al., 1993). In volcanology, it has been found to hold for the lengths of intervals of eruption rates exceeding various thresholds (Dubois and Cheminée, 1991; Sornette et al., 1991). Power law number and probability distributions can arise in a qualititatively different way in scale invariant fields. The field (rather than geometric sets of points) may have intensity fluctuations which are algebraically distributed: "self-organized criticality" (s.o.c; Bak et al., 1987). The most celebrated geophysical example of this is the distribution of seismic intensity, the "Gutenberg–Richter law" (Gutenberg, 1944; see Schertzer and Lovejoy, 1994, 1996) for a recent review of such behaviour in turbulent geophysical systems).

Returning to vesicle size distributions, various functional forms are routinely used for performing empirical regressions. The functional forms for the statistical fits are usually chosen on the basis of homogeneity assumptions. Different samples are fit and the variations in the parameters are then used to infer sample-to-sample differences. The differences in the fitted parameters are usually then used to infer spatial and/or temporal heterogeneity. Unfortunately the usual distributions are not invariant under "mixing". For example in the case of vesicles, two samples with exponential vesicle distributions with identical characteristic volumes may undergo different degrees of expansion due to different pressure and temperature conditions and hence evolve to different characteristic volumes. It will then be unlikely that genuine exponential behaviour ever be observed since any mixing of the two samples would lead to a non exponential result.

On the other hand power law number densities (Eq. (1)) have the important feature that if two samples with identical exponents (B) but different V^* values are mixed, then the exponent is conserved for the resulting mixture. Furthermore, under fairly general circumstances, if V equals the sum of a large number of random contributions, its density will tend to a "universal" limit, the "Levy distribution" (this is the "generalized central limit theorem" of probability theory). A consequence of this theorem is that when the individual random variables

[1] the number of vesicles with size between V and $V+dV$ per unit volume of lava. As expressed in Eq. (A.2) the number density is the derivative of the number distribution.

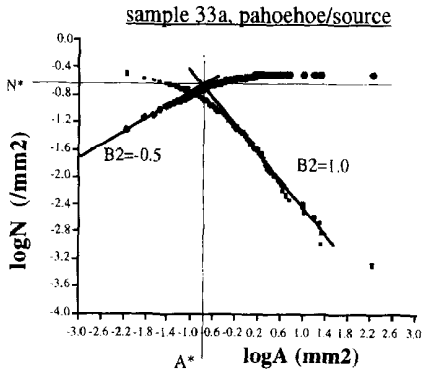
sample 33a, pahoehoe/source
N*
B2=-0.5
B2=1.0
A*
logN (/mm2)
logA (mm2)

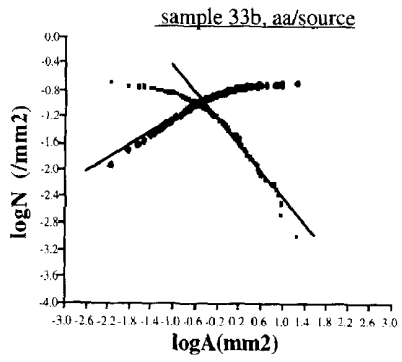
sample 33b, aa/source
logN (/mm2)
logA(mm2)

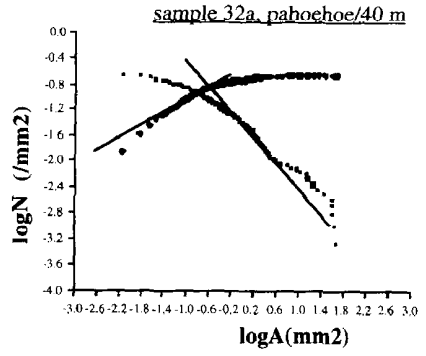
sample 32a, pahoehoe/40 m
logN (/mm2)
logA(mm2)

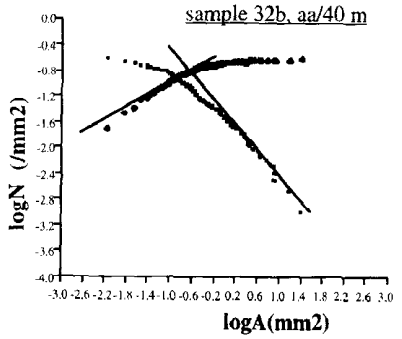
sample 32b, aa/40 m
logN (/mm2)
logA(mm2)

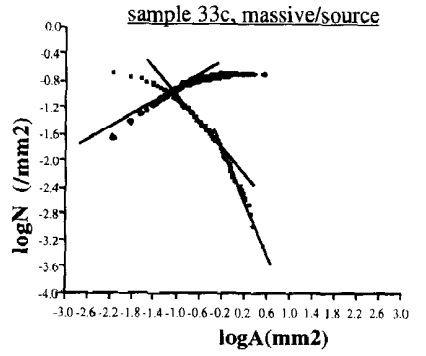
sample 33c, massive/source
logN (/mm2)
logA(mm2)

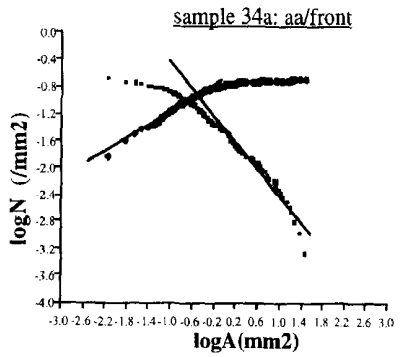
sample 34a: aa/front
logN (/mm2)
logA(mm2)

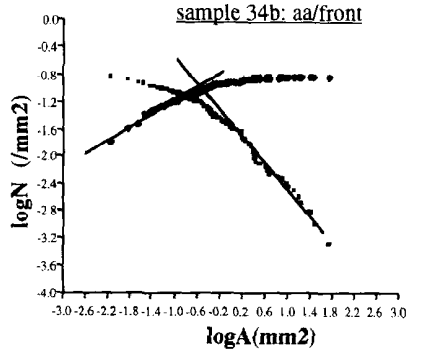
sample 34b: aa/front
logN (/mm2)
logA(mm2)

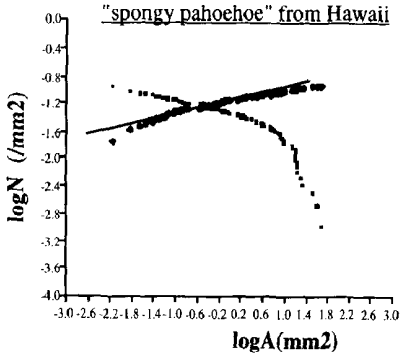
"spongy pahoehoe" from Hawaii
logN (/mm2)
logA(mm2)

have power law tails with $B < 2$, the limiting sum has the same exponent, whereas for $B > 2$, the limiting result is a non algebraic function, the familiar gaussian. The special case $B < 2$ thus leads under addition to the conservation of the exponent B: this range of B is relevant here. A final argument in favour of power law distributions is that, during the 1980's, advances in the study of non-linear dynamical systems has shown that such systems generally (although not necessarily) lead to power law distributions ("non classical s.o.c."; Schertzer and Lovejoy, 1987, 1996).

3.2. Relationship of the vesicle number distribution from one space to another

Understanding vesicle dynamics requires knowledge of their distribution in three-dimensional space; unfortunately most analyses (including ours) are over subspaces. It is therefore important to determine the general relation between distributions in spaces of various dimensions. Many authors (e.g., Sarda and Graham, 1990; Mangan et al., 1993) have used highly restrictive formulae which only apply to spherical vesicles. In Appendix A, using only the much weaker restriction of statistical isotropy (which allows individual vesicles to have arbitrary shapes, only on "average" need they be spherical), we derive the general transformation rules (even this can be extended to statistical anisotropy, as long as the latter is still scaling). These are particularly simple in the case of power law distributions, since the exponents for different spaces will then be linearly related.

The special cases relevant for our work are obtained using Eqs. (A.5) and (A.6):

$$B_3 = \tfrac{2}{3}B_2 + \tfrac{1}{3} \quad (2)$$

$$B_1 = 2B_2 - 1 \quad (3)$$

which relates the measured vesicle area exponent B_2 to the volume exponent B_3 and length exponent B_1, respectively [2]. Subscripts indicating the dimension of the sampling space will be used whenever necessary. An exponent B without a subscript will generally correspond to volumes (three-space) although occasionally—this will be obvious from the context—it may refer to any dimensional ("d-volume", i.e., volume, area, length, etc.).

3.3. Size distributions of vesicles through analysis of individual samples

Power law number densities such as Eq. (1) have the property that, depending on the exponent, they imply divergences in the total number of vesicles per unit volume in the small volume limit ($B > 0$), in the large volume limit ($B < 0$), or at both limits ($B = 0$). Similarly, the related vesicularity distribution P will diverge or converge for large V depending on whether B is less than, equal to or greater than 1. These divergences mean that pure power laws can, at best, only be models of the vesicle distribution over a range greater than an inner scale or less than an outer scale beyond which they will break down. Because of these cut-offs and the necessity for the total vesicularity (denoted P^* below [3]) to be bounded between 0 and 1, we distinguish between five qualitatively distinct cases. They are discussed in Appendix B.

The vesicles for Mount Etna lava samples illustrate several of these cases. In each sample, we will find the number–size distribution functions N are a composite form of two of these cases, with the small

[2] It is perhaps worth noting the interesting property of $B_2 \approx -0.5$, as estimated empirically later for the diffusion regime. This leads to $B_3 \approx 0$, which in fact corresponds to a volume number density uniform in $\log V$ (see Appendix B, case $B = 0$).

[3] which corresponds to the ensemble mean vesicularity calculated over an infinite number of statistically identical samples, in distinction to the sample vesicularity P_s calculated over one (finite) sample.

Fig. 5. Plots of the number of vesicles of size larger and smaller than A (A in pixels), $N(A' > A)$, $N(A' < A)$ versus A. Samples 32a, 32b, 33a, 33b, 33c, 34a, 34b are shown as examples. Slopes $+0.5$ and -1.0 are shown for all samples ($B_2 = -$slope). Slope -2.0 is also shown for 33c. For comparison, the Hawaiian spongy pahoehoe is plotted with slopes of $+0.2$. All logs are base 10.

and large size regimes involving different exponents. In Fig. 5, we express the number distribution of the vesicle sizes for the 1985 overflow series (32–34 samples, Table 2). $N(A' > A)$ versus A is the number of vesicles larger than the vesicle area A, and $N(A' < A)$ versus A is the number of vesicles smaller than A (A in mm^2). These numbers are both normalized to their related digitized sample surface (number/mm^2). Log–log plots are used since power laws will be linear.

The direct use of vesicle areas rather than "radii" avoids any assumptions about the shapes of the vesicles. The reason we must plot both $N(A' < A)$ and $N(A' > A)$ is due to the fact that there are two regimes, one with $B_2 > 0$ and the other with $B_2 < 0$ (see Appendix B). Data points from 33a and 33b samples follow a linear trend on log–log plots with $B_2 \approx 1.0$ ($B_2 = -$slope; $B_3 \approx 1.0$) for sizes larger than A^*, and another linear trend close to $B_2 \approx -0.5$ ($B_3 \approx 0$) for sizes smaller than A^*. In the smallest sizes, the linear log–log regression is less good, perhaps due to the resolution limit of our digitization. The two power law regimes we can recognize correspond to:

$$N(A' < A) = N^* \left(\frac{A}{A^*} \right)^{-B_2} \quad A \leq A^*, \text{ for } B_2 < 0$$

$$N(A' > A) \approx N^* \frac{A^*}{A} \quad A \geq A^*, \text{ for } B_2 = 1$$

where N^* is the number distribution of vesicles at the transition point. A^* is the outer limit of the small vesicle regime ($B_2 < 0$), and the inner limit for the large vesicle regime ($B_2 = 1$). The "$\approx$" sign in the second equation indicates equality to within slowly varying (e.g., logarithmic) factors as discussed in Appendix B. Both linear fits intersect in a region—called a transition zone—characterized by A^* and N^* values. In this zone data deviate from both linear trends.

As discussed in Appendix B (Eq. (A.11a)), all the vesicles in a $B_2 = 1$ regime contribute significantly to the total vesicularity. In contrast, in $B_2 < 1$ regimes the main contribution comes from the large vesicles.

Table 2
Values of the transition zones of the samples. See text for explanations

Sample (No.)	Fractal C	A^* (mm^2)	l_1/l_2 (mm)	N^* (mm^{-2})	A^*N^*	A_s (mm^2)	P_2 (%)
01c	0.62	0.16	0.09/3.5	0.251	0.040	15.0	13.7
07a	0.54	0.25	0.27/3.5	0.126	0.031	58.5	19.3
01b	0.57	0.40	0.17/3.5	0.079	0.032	64.0	15.7
02b	0.58	0.25	0.17/3.5	0.126	0.031	45.5	17.1
Spongy	0.23	6.31	0.09/3.5	0.100	N.A.	47.5	50.7
23i	0.64	0.50	0.27/3.5	0.079	0.040	20.5	16.3
22a	0.64	0.25	0.27/3.5	0.159	0.040	22.0	19.7
22c	0.89	0.40	0.27/6.9	0.040	0.016	7.04	5.2
32a	0.41	0.25	0.17/3.5	0.159	0.040	47.0	29.9
32b	0.60	0.25	0.09/3.5	0.159	0.040	25.5	16.2
33c	0.91	0.10	0.09/3.5	0.126	0.013	3.5	3.8
33a	0.47	0.16	0.17/2.2	0.199	0.032	180.5	27.5
33b	0.63	0.40	0.27/3.5	0.100	0.040	17.5	17.2
34a	0.54	0.32	0.17/3.5	0.126	0.040	30.5	19.1
34b	0.56	0.25	0.17/3.5	0.100	0.025	56.5	17.5
46b	0.50	1.26	0.27/3.5	0.079	0.100	28.5	24.8
46c	0.38	1.58	0.27/3.5	0.050	0.079	160.0	35.0
46a	0.38	2.00	0.27/3.5	0.032	0.063	100.5	33.4
45	0.32	1.58	0.27/3.5	0.063	0.100	60.5	41.5
58c	0.59	0.50	0.69/8.7	0.050	0.025	185.5	12.6
58b	0.77	0.13	0.17/5.5	0.126	0.016	30.0	6.3
58a	0.57	0.40	0.17/3.5	0.079	0.032	24.5	16.9
58d	0.47	0.79	0.27/5.5	0.079	0.063	26.5	22.8

The third sample collected at the source of the overflow, the massive pahoehoe (33c), suggests an additional linear trend: $B_2 > 1.0$ for the largest sizes (actually, it is over too narrow a range to be conclusive). Since in regimes with $B_2 > 1$ the main contribution to the vesicularity is from the smallest vesicles, the vesicularity of sample 33c is determined primarily by vesicles in the range limited by the A^* value and the break in a slope from $B_2 = 1$ to $B > 1$, i.e., between 0.10 and 0.63 mm^2 (Table 2). The two samples collected 40 m from the source of the overflow (32a, 32b) and the two samples from the front (34a, 34b) show approximately the same pattern as 33a and 33b. Sample 32a also demonstrates that the number distribution of large vesicles fluctuates around the linear trend, which is expected because of the statistical variability. Finally, the transition zone has variable N^* and A^* values, and is more or less wide according to the considered samples (compare 33b and 32b for example).

The overflow series exhibits the same power laws we find in all other series (table 2 and appendix III in Gaonac'h, 1994). Note that A^* and N^* values vary from one sample to another, and the product N^*A^* also varies from sample to sample (Table 2), increasing with higher observed vesicularity P_2. We will examine this in more detail in Section 3.5. Only three samples (33c, 46b, 22c) have $B_2 > 1.0$ for large vesicles; however, we need more data to confirm this tendency. In comparison, the Hawaiian spongy pahoehoe (Fig. 5) exhibits a unique general trend of $B_2 = -0.2$ ($B_3 = 0.2$) slope for most of the size range with the positive slope extending to the largest vesicles.

Vesicle growth mechanisms and vesicle populations can be identified by statistical analysis, as previously documented (e.g., Toramaru, 1990). The existence of two separate scaling regimes—similar from one sample to another—with distinct exponents suggests two different vesicle growth regimes associated with different predominant scaling growth mechanisms. In Gaonac'h et al. (1996), we proposed a model in which the small vesicle regime corresponds to a range of scales where diffusion is dominant whereas the large vesicles regime may correspond to the dominance of a coalescence mechanism. The transitional zone is thus a range of scales where both growth mechanisms are important. A simple cascade coalescence model—with the assumption that the gas volumes are conserved by the coalescence process—theoretically yields a value of $B \approx 1$ (Gaonac'h et al., 1996). Hence our empirical results support the cascading coalescence model of successive vesicle collisions of larger and larger volumes with fewer and fewer vesicles acting at each step in the collision cascade. We further suggest that the scaling regimes have cut-offs associated with the transition zones and values (A^*, N^*). In this framework, the different A^* and N^* values correspond to different volcanological conditions and samples histories (initial dissolved gas content, eruption temperature, cooling rate, etc.). The very different Hawaiian spongy pahoehoe size distribution suggests that the corresponding vesicle growth mechanism is very different compared to the Etna lavas. This result is consistent with the static coalescence growth process suggested by Walker (1989).

3.4. Size distributions of the normalized ensemble: refined estimates

Using the vesicle distributions from the samples available here (which typically have only 100–300 vesicles, and a corresponding scaling range of areas of factors $\approx 10^2$–10^3), it is not possible to obtain very precise estimates of the exponent (or in the case $B = 1$, to obtain the exact form of the slowly varying corrections to the V^{-1} law; see Appendix B for further discussion). In order to more fully test the scaling hypothesis and to obtain more accurate estimates of the exponents, we therefore seek to combine all the samples into a single histogram. We normalized each sample using the values A^* and N^*; this is necessary to remove the effect of geological differences between the samples (if the scaling regimes were infinitely wide, this would not be necessary). Fig. 6a demonstrates the result showing power law trends identified by linear regression in log plots, with the two different regimes corresponding to those found in the individual plots. The normalized plot has a B_2 of ≈ -0.40 ($B_3 \approx 0.05$) for small vesicles, and B_2 of ≈ 0.80 ($B_3 \approx 0.85$) for large vesicles, which are in fact quite close to the two-dimensional values mentioned above which were crudely estimated for individual plots (≈ -0.5; ≈ 1.0). Fig. 6b exhibits the normalized distribution of

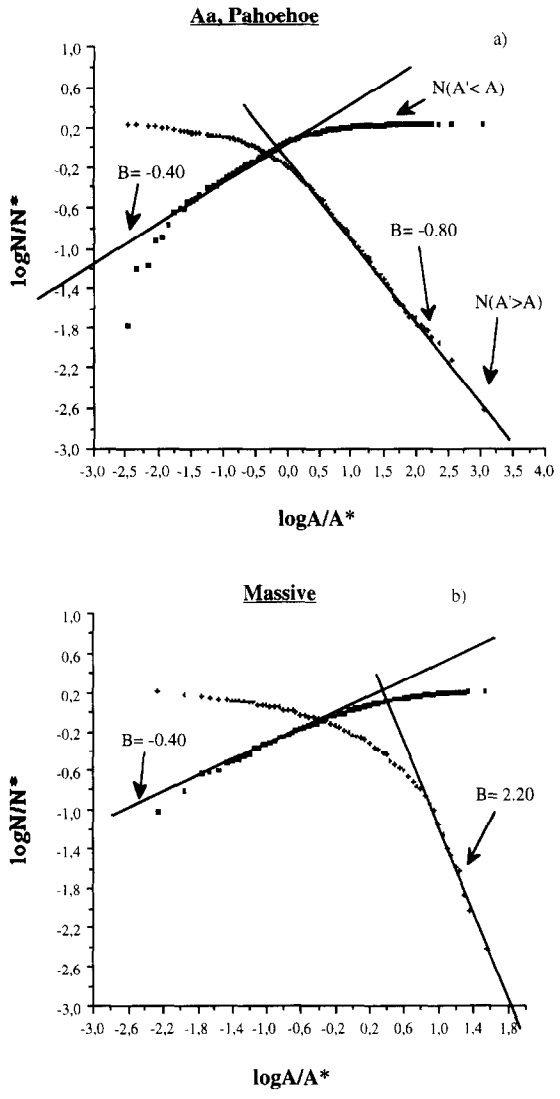

Fig. 6. (a) Plot of the number of vesicles of size larger and smaller than A (A in pixels), $N(A' > A)$, $N(A' < A)$ versus A normalized to A^* and N^* for samples 01c, 17a, 01b, 02b, 23i, 22a, 32a, 32b, 33a, 34a, 33b, 34b, 46c, 46a, 45, 58c, 58b, 58a, 58d, all together. (b) Same plot for samples 33c, 46b, 22c.

the samples with individual slopes having $B_2 > 1$ for large vesicles. Theoretically, Gaonac'h et al. (1996) explained values slightly below 1 by some degree of nonconservation of volume during the cascade or alternatively due to some small contribution to vesicle growth from noncoalescence mechanisms. Specifically, a value $B_3 \approx 0.85$ corresponds to a contribution of $\approx 10\%$ from such mechanisms.

3.5. Sampling properties

We have already mentioned that when $B = 1$ the entire large vesicle range is important for determining the total vesicularity; when $B < 1$ the largest will dominate. However, in either case, the true extent of the range will not be evident since the largest vesicle size observable will vary substantially even among neighbouring samples due to the slow fall-off in the number distribution. When such variations in the total vesicularity are observed, we cannot *necessarily* conclude that the different samples had fundamentally different volcanology/history; the differences could be due to the large random fluctuations and cannot be avoided in the collection process. If the model is valid then the appropriate characterization of the geological sample-to-sample differences will be the parameters N^*, V^* (as estimated by fitting the entire distribution).

To understand this in more detail, consider the case $B = 1$. Using the approximation $N(V' > V) \approx N^* V^*/V$ (Eq. (A.12b)), we can estimate the dependence of the largest vesicle (V_s), and hence vesicularity, on the volume v_s of the sample ("s" for "sample"). The following argument is analogous to that used to estimate the maximum order of singularity present in finite samples of multifractal fields (Schertzer and Lovejoy, 1989). For the moment, we only consider the contribution to the total vesicularity of the sample P_s from the $B = 1$ coalescence regime, P_c (this is the major contribution to the total vesicularity, see below and Gaonac'h et al., 1996). First, the total number of vesicles in the sample is simply the total number per unit volume (N^*) multiplied by the sample volume (v_s):

$$N^* v_s$$

The ensemble probability—over an infinite number of samples—corresponding to the largest vesicle of volume V_s is:

$$Pr(V' > V_s) = \frac{N(V' > V_s)}{N^*} = \frac{V^*}{V_s} \tag{4}$$

We now use the fact that in a sample of $N^* v_s$ vesicles, the largest vesicle has a probability of occurrence $\approx 1/(N^* v_s)$ (the sample frequency of occurrence is used to estimate the ensemble fre-

quency of occurrence). V_s can therefore be estimated as:

$$V_s \approx N^* V^* v_s$$

For fixed N^*, V^*, the largest vesicle in the sample is therefore expected to increase linearly with sample volume (generalizations for $B \neq 1$ are given below). Of course, this estimate is only statistical; V_s will actually be a random variable whose typical value is given by the above expression. Finally, the contribution to the sample vesicularity due to coalescence P_c will be given by integrating $Vn(V)$ $[= V(dN/dV) = (N^* V^*/V)]$ over the size range of V^* to V_s:

$$P_c = \int_{V^*}^{V_s} \frac{N^* V^*}{V} dV = N^* V^* \ln \Lambda \approx N^* V^* \ln N^* v_s \quad (5a)$$

where $\Lambda = V_s/V^*$. Unless the sample size is very large, P_c will be less than P^*. Of course, the $N(V' > V) \approx V^{-1}$ approximation will break down for large enough sample volumes v_s (specifically, when $P_c \approx P^*$). Indeed, considering the two-dimensional situation (with a_s the sampling area corresponding to v_s, A_s to V_s), we can consider the limit of large a_s such that $P_s = P^* = 1$: this limit corresponds to $N^* a_s \approx \exp(1/N^* A^*)$. For $N^* A^*$ (here $\approx 0.04 \pm 0.02$), it will not be important for linear dimensions smaller than $\sqrt{a_s} \approx 10^2$ m. For smaller samples, the breakdown will not be reached, and the vesicularity will depend on v_s in the manner described by Eq. (5a)a.

When $B \neq 1$, the formula corresponding to Eq. (5a)a is:

$$P_c = N^* V^* \frac{B}{1-B}\left(\frac{\Lambda - \Lambda^B}{\Lambda^B - 1}\right) \quad (5b)$$

with $\Lambda > 1$. Note that this reduces to Eq. (5a)a in the limit B tends to $\Lambda \gg 1$. In both Eq. (5a) and Eq.

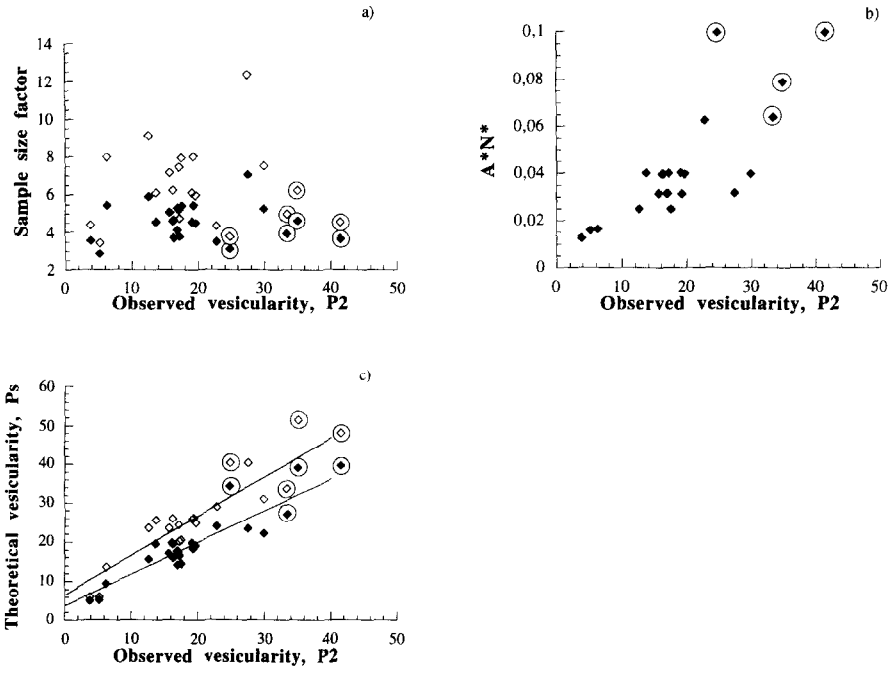

Fig. 7. (a) Plot of the sample size factor P_c/N^*A^* as expressed in Eq. (5a) and Eq. (5b) [respectively log Λ, for $B_2 = 1.0$ (♦) and $(0.8/0.2)(\Lambda - \Lambda^{0.8}/\Lambda^{0.8} - 1)$ for $B_2 = 0.8$ (◇)] as a function of the observed vesicularity P_2. The four values of the collected initial 1985 source samples are identified by circles around the diamonds. (b) Plot of the volcanology/history factor A^*N^* for all samples — determined as the transition points from the intersection of the diffusion and coalescence regime regressions — versus P_2 (see Table 2). (c) Theoretical versus observed vesicularities $P_s = P_d + P_c$. Same symbols as in (a). Linear regressions are shown for the two cases, -0.5/1.0 and -0.40/0.80, calculated for the 19 samples without large vesicle breaks ($B_2 > 1$). A slope 1 associated with the refined values -0.40/0.80 indicates that the theoretical values are unbiased vesicularity estimates; P_g associated with the values -0.5/1.0 gives only a 0.8 slope versus P_2.

(5b), P_c is the product of two factors, the first ($N^* V^*$) is dependent only on the volcanological characteristics/vesicle history, while the second (involving V_s) is sensitive to the sample. Note that when $B > 0$, $\Lambda \gg 1$, we have $P_c \approx N^* V^* [B/(1-B)](\Lambda^{1-B} - 1)$. When $B < 1$, this is sensitive to Λ whereas when $B > 1$, $P_c \approx N^* V^* B/(B-1)$ which is independent of Λ as expected.

When considering the two scaling regimes, we observed that they intersect in a transition zone defined by A^* and N^* values. The two values vary from sample to sample, suggesting volcanological differences such as a higher dissolved gas content in samples with a higher N^*. On the other hand, the product $N^* A^*$ also varies from one sample to another; we consider this variation now as a function of the total sample vesicularity. While in Eq. (5a) and Eq. (5b) we neglected—for simplicity—the diffusive term P_s, we will consider it now so as to compare theoretical and observed vesicularities. The total theoretical sample vesicularity, taking into account $B_d < 0$ for the diffusion regime and $B_c \leq 1$ for the coalescence regime (see Eq. (A.10b) and Eq. (5b)) is therefore $P_s = P_d + P_c$ with P_d given by:

$$P_d = N^* A^* \frac{B_d}{B_d - 1} \tag{6a}$$

i.e.:

$$P_s = N^* A^* \left[\frac{B_d}{B_d - 1} + \frac{B_c}{1 - B_c} \left(\frac{\Lambda - \Lambda^{B_c}}{\Lambda^{B_c} - 1} \right) \right] \tag{6b}$$

where $\Lambda = A_s/A^* > 1$ for the areas (when $B_c = 1$, Eq. (5a) should be used for P_c). P_s being small ($B_d = 0.5$, $B_d/(B_d - 1) = 1/3$ which corresponds to less than 10% of the total P_s, see Gaonac'h et al., 1996), we expect the approximation Eq. (6b) to be close to the total theoretical vesicularity. To make the comparison, we consider two cases: the first involves the exponent area values found in individual samples, -0.5 and 1.0, respectively, for the small and the large vesicle regimes; the second involves the refined area values of -0.40 for the small vesicles and $B \approx 0.80$ for the large vesicles.

First consider the behaviour of the sample dependent factor. In Fig. 7a, the observed vesicularity P_2 does not show any systematic variation with the sample size factor [$\log \Lambda$, and $(0.8/0.2)(\Lambda^{0.8})/(\Lambda^{0.8} - 1)$, for $B = 1$ and $B = 0.8$, respectively]. In contrast, considering the history/volcanology factor $N^* A^*$, Fig. 7b shows that the samples are systematically more vesicular for higher $A^* N^*$ values. This is in agreement with the hypothesized random sample to sample variability present in the former factor but absent in the latter. Also shown in Fig. 7 are the four cases found near the initial 1985 source which have particularly large vesicularity. Their lower A_s/A^* values (full and open diamonds with circles) can be explained due to a lack of time for these samples to have developed large enough vesicles to reach a large A_s/A^* ratio. Data from Fig. 7c confirm that the theoretical expression of the total sample vesicularity as expressed in Eq. (6b) is a very good approximation to the observed data and may be used in future models. Moreover, Eq. (6b) with the refined exponents confirms that the $-0.40/0.80$ values are more accurate (they yield a slope ≈ 1 in Fig. 7c, implying no theoretical bias) than the $-0.5/1.0$ values (slope ≈ 0.8). From Fig. 7, we can therefore distinguish sources of variability in the lava vesicularity: a sample to sample variation of the vesicularity associated with the presence or absence of a single large vesicle, and a systematic variation dependent on the product $N^* A^*$. The systematically large vesicularity of the initial 1985 source samples can therefore be explained by the higher $N^* A^*$ values.

3.6. The scale invariance of vesicle patterns when $B = 1$

We now consider the implications of the distributions for the scaling of vesicle regions (i.e., the spatial pattern rather than the number distribution of the voids). To understand the special character of the $B = 1$ distribution [4], we will initially consider the scaling with arbitrary $B > 0$. Consider a spatial magnification operation of a factor λ on a lava sample with $N(V' > V)$, the number distribution of the enlarged sample is related to the original distribution by:

$$N(V' > V) = \lambda^d N_\lambda(V' > \lambda^d V) \tag{7}$$

[4] Even if $B \approx 0.85$ rather than 1, the following discussion will be a relevant approximation over the finite range of scales observed.

The λ^d factors (in a d-dimensional sampling space, the V values are "d volumes") account for the increase by factors λ^d of the volume of both the samples, and the vesicles. The power law form and exponent of the enlarged distribution is thus the same, but the amplitude is rescaled as follows:

$$N_\lambda^* = \lambda^{d(1-B)} N^* \tag{8}$$

This rescaling corresponds to the fact that the relative density of large and small vesicles is the same before and after the enlargement, but the overall number density is increased or decreased depending on whether $B > 1$ or $B < 1$. It is only in the special case $B = 1$ that the number density is completely invariant ($N_\lambda^* = N^*$, i.e., independent of λ). Therefore, it is only in this case that (assuming statistical isotropy) the enlarged pattern of vesicles will be statistically identical with the original; the vesicle pattern will be "self-similar" (this result can be generalized to anisotropic, non-self-similar, scaling using Generalized Scale Invariance; Schertzer and Lovejoy, 1985). In summary, whatever the value of B, the volume distribution is scaling, and the exponent B is scale invariant. However, when $B = 1$, we have the additional property that the actual pattern is also scale invariant. This means that in this case, it is possible over the corresponding scale range to find fractal structures (over limited ranges of scales, this will be approximately true if B is only approximately 1). Indeed, the empirical evidence presented in Section 4. indicating the scaling of box-counting over scale ranges comparable to those where $B \approx 1$ is observed supports the $B \approx 1$ hypothesis.

4. Scaling properties of the spatial vesicle patterns

4.1. Resolution dependence

If $B_3 \approx B_2 \approx 1$, the structures will be fractal over some range, and hence the estimate P_2 will vary as a function of the resolution of the analyses. A higher resolution ($l < 0.085$ mm) would provide more details on the complex shapes of vesicles.

If we expect scale invariance of the vesicle pattern (i.e., the points on the matrix are fractal sets over a range of scales), the number $N_b(l)$ of l sized vesicle pixels ("boxes") needed to cover the vesicle distribution will be related to the resolution l as:

$$N_b(l) \propto l^{-D} \tag{9}$$

which—recalling that $N_b(l)$ is defined by unit area —is equivalent to:

$$P_2(l) \propto \frac{N_b(l)}{l^{-d}} \propto l^C \tag{10}$$

where D is the fractal dimension, d is the dimension of the observing space, and $C = d - D$ is the fractal codimension (C will be the linear slope of $\log P_2(l)$ versus $\log l$). For datasets embedded in two-dimensional cross sections, $d = 2$ and $0 \le D \le 2$, $0 \le C \le 2$. In the case where $D = d$, $P_2(l) \propto$ constant, implying that $P_2(l)$ is constant at all resolutions. C is the exponent relating the fraction of vesicles to the resolution l. For a very large isotropic sample, we expect to have the same vesicles fraction whether the latter is estimated from volumes, areas or lengths; hence in this sense, C is dimensional invariant.

4.2. Fractal codimension

The estimate of the fractal codimension of each sample was performed by using the box counting method (see Falconer, 1990), which is commonly used for estimating the fractal dimension of strange attractors associated with non-linear chaotic dynamical systems. We obtained a series of areal fractions corresponding to P_2 as functions of resolution (Fig. 8). λ, P_2 are non-dimensional as P_2 and corresponds to the ratio of largest possible box length ($l_o = 512$ pixels) to the length l in pixels ($512/l$). Sample 32a exhibits a linear trend from an inner limit $l_1 = 0.17$ mm to an external limit $l_2 = 3.50$ mm pixels with $C \approx 0.41$ (i.e., $D = 2 - 0.41 = 1.59$), indicating a scaling behaviour of the vesicularity over a scale range of 2^5. We repeated the measurements for several samples and found a variation of ± 0.06 for D. As expected, the breakdowns of the scaling roughly correspond to those of the $B = 1$ regime (recall that the value $B = 1$ is invariant with respect to subspaces, see Appendix A), although the ranges are somewhat offset towards the small vesicles. At low resolution ($\log \lambda < 1.1$; $l > 3.50$ mm), the vesicularity is no longer dependent on the resolution l. At high resolution, the end of linearity occurs at a

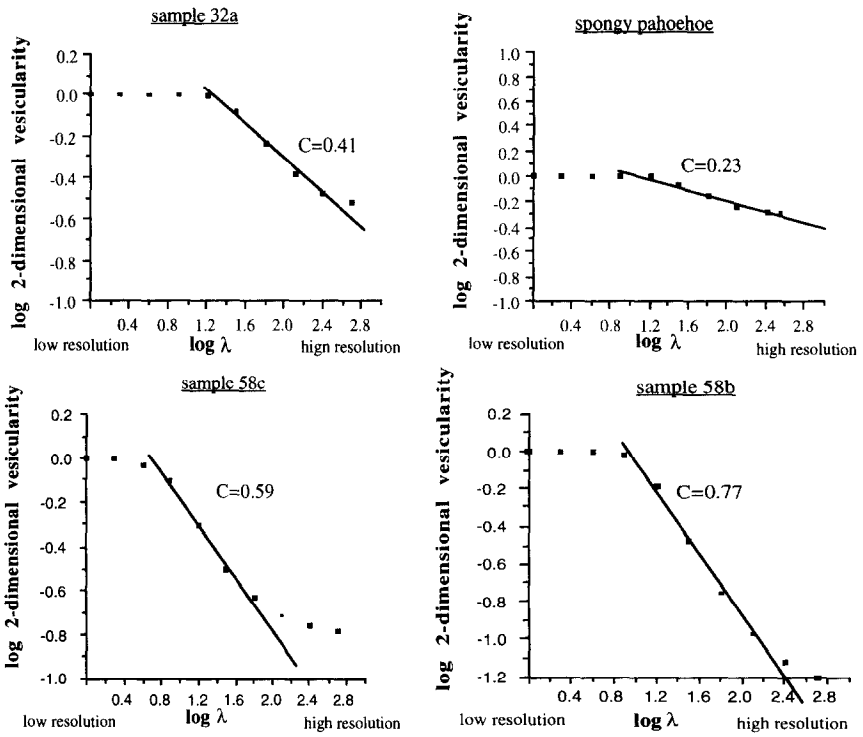

Fig. 8. Plot of log P_2 versus log λ for samples 32a, the spongy pahoehoe, 58c and 58b. C is the fractal codimension of the linear trend between—e.g., in the 32a case—log $\lambda = 1.1$, corresponding to $l_2 = 512/\lambda = 41$ pixels = 3.50 mm, and log $\lambda = 2.4$ corresponding to $l_1 = 512/\lambda = 2$ pixels = 0.17 mm.

resolution close to 1 pixel (0.085 mm). Since this resolution is close to the smallest detectable vesicles in thin sections (0.1–0.2 mm), it may be the true inner limit. Here, we require more data to confirm this tendency at higher resolution. Results in Fig. 8 imply that when measuring vesicularity, the resolution at which it is estimated has to be known; going back to sample 32a, $P_2(l) \propto l^{0.41}$. For resolution lower than 3.50 mm, the vesicularity estimated this way is at its maximum, 100%, while at high resolution (smaller pixel length), the vesicularity decreases to $\approx 30\%$ as vesicle irregularities are increasingly taken into account. This 100% result is because box-counting is an all or nothing method. However, this is adequate for studying the scaling and gives similar results to other techniques such as correlation integrals and dimensions.

When comparing the log $P_2(\lambda)$ − log λ plots for all samples (appendix II in Gaonac'h, 1994), we can identify a similar linear trend with an external limit l_2 varying from 2.20 to 8.70 mm. The external limit was always within the available size range (between 0.085 and 43.52 mm) and was readily detected. It corresponds to the largest vesicle sizes encountered. Inner limits l_1 exhibit the same problem as in sample 32a. The samples have fractal codimensions ranging between 0.70 and 0.30 (dimensions between 1.30 and 1.70), except for the massive lavas (22c, 33c, 58b) which have lower D regions (the vesicles are "sparser"). P_2 of the Hawaiian spongy sample with a D value approaching 1.8 (Table 2 where $C = 2 - D$) cannot be considered fractal since D approaches 2; this is in accord with our estimate $B_2 \approx -0.2$ which is significantly less than 1.0.

It is perhaps worth noting in this connection that there is a certain amount of mathematical theory about random "cut-outs" or "tremas" (see Mandelbrot, 1983, for a review and discussion). These are stochastic processes constructed by taking a collection of elementary geometrical shapes whose distribution as a function of size is V^{-1}. When these shapes are randomly placed, they tend to overlap. If

we consider that they "cut out" regions of the embedding space, then when the distribution V^{-1} is continued to infinitely small scales, the remaining (non cut-out) regions are fractal sets. A somewhat surprising feature, which is a consequence of the special role of $B = 1$, is that the fractal codimension of the remaining set depends linearly on the prefactor in the size distribution (hence on the history factor $N^* V^*$).

If this process corresponds to the distribution of gas vesicles, then in the limit, the overall vesicularity would approach the unity with a fractal set (volume approaching zero) remaining. Recalling that the total vesicularity is mostly determined by the product of the sample and the history factor $N^* V^*$ (Eq. (5a)), we may thus expect a correlation between the total vesicularity and the fractal dimension of the remaining of the vesicles. In fact, Fig. 4b shows that, for vesicularity higher than 10%, P_2 estimated at the highest available resolution, 300 dots per inch (dpi), is positively correlated with the fractal dimension D of the vesicles. Hence, we are able to find similar properties between C and $N^* V^*$ than for "cut-outs", but in the present case, C corresponds to the vesicles set, the vesicle-free regions representing > 50% of the total surface of a sample, and thus not varying much according to the resolution (as expected for fractals).

5. Discussion and conclusion

In this paper we have proposed a scaling framework for analysing and modelling vesicle distributions in lava. This was justified by basic empirical and theoretical considerations: the observation that even small lava samples commonly displayed enormous ranges of vesicle volumes (factors of a million are routine), coupled with the absence of characteristic sizes in any of the known mechanisms of vesicle formation (diffusion, expansion, coalescence). Rather than proposing ad hoc regressions — or simplistic characterizations of such broad distributions by mean or median vesicle sizes — this scale invariant framework predicts power law distributions (these — and log corrections — are the only distributions without characteristic scales). A scale invariant framework was also considered attractive since it has been generally quite successful in geophysics (accounting notably for the ubiquity of fractal structures, multifractal statistics and power law distributions in geophysics). Specifically it has also provided a surprisingly accurate account of lava morphology over wide ranges of scale (Gaonac'h et al., 1992; Bruno et al., 1992).

The predicted power law densities $[n(V) \approx V^{-B-1}]$ have several peculiarities (due to either small and/or large V divergences) which we carefully outlined. In particular, since probabilities and vesicularities must be well defined between 0 and 100%, this leads us to divide such distributions into five subclasses; in each we indicate how the exponents can be empirically estimated. This includes the comparison of cumulative number distribution functions for both the number of vesicles exceeding a fixed threshold, as well as — perhaps for the first time — the number less than a fixed threshold. A second theoretical point is that although power law number distributions are themselves scale invariant, the associated spatial distributions of vesicles will generally not be scale invariant (fractal). The only exception is when $B = 1$, a value close to that observed for the large vesicles. It is only in this case that the spatial vesicle pattern will define fractal sets; a prediction we confirm using a box counting algorithm. Finally, for exponents less than 1, the vesicularity is mostly determined by the largest one or two vesicles in the sample (even though the vast majority of the vesicles are small). This leads to large sample to sample vesicularity fluctuations — even if the lava samples have identical volcanological characteristics.

The scaling framework has another advantage; it enables us to develop formulae relating the distribution measured on one subspace (here planar cross sections) to that of another (here the volume distributions). This enables us to avoid restrictive assumptions of vesicle sphericity and the complex "corrections" sometimes used for estimating volume distributions from cross sections. Our technique, coupled with an original — and simple — method of sawing, painting and digitizing lava samples enabled us to study many more samples than just the ones containing spherical vesicles.

Results of our analysis of vesicle size distributions of Mount Etna confirm that they are characterized by power laws. We find two distinct regimes: a

small-scale regime (with an area exponent $B_2 \approx -0.5$ equivalent to a volume exponent $B_3 \approx 0.0$) as well as a large-scale regime (with $B_2 = B_3 \approx 1$) with transition vesicle area scale A^* and density N^* which we argue capture the volcanologically significant sample to sample differences. Refined exponent values are $B_2 \approx -0.40$ ($B_3 \approx 0.05$) and $B_2 \approx 0.80$ ($B_3 \approx 0.85$), respectively, for the small and large vesicle regimes. The results also determine the limits of the two scale invariant regimes. Table 2 shows these characteristic sizes and parameters established from the different samples. Considering vesicles from the 1985 and 1991—1993 lavas we find that aa and pahoehoe were not different, nor were samples from horizontal and vertical sections. For sizes smaller than A^*, the vesicles have smooth rounded boundaries whereas for sizes larger than this—as theoretically predicted—they are fractal (we estimate the corresponding dimensions). An important implication of our findings is that although lavas are classified into different types according to their morphology, they have similar statistical behaviour related to their vesicle size distributions.

Although—along with Mangan et al. (1993)—we find that the small vesicles are far more numerous than the large ones, contrary to them, we find that their relative contribution to the total vesicularity is nearly negligeable. This is because the long tail on the number distributions implied by $B \approx 1$ means that a few very large vesicles will dominate the vesicularity. Large variation of the vesicularity of a lava flow will affect for example the relative viscosity or the compressibility of the flow and may lead to strong non linear rheological behaviour of the flow. Vesicles a few meters in size (as observed for example by Blackburn et al., 1976) reveal extreme rheological behaviour. Because of the large sample-to-sample variations implied by $B \approx 1$ (which may hide a variation of A^*, N^* from the source to the lava front) the study of larger surfaces will yield even larger vesicles which will strongly affect the total vesicularity.

The presence of two different scaling regimes, systematically observed in each collected sample leads us to suggest that these regimes are associated with two different vesicle growth regimes where diffusive processes may be involved in the small vesicle growth, and a dominant coalescence mechanism may be involved in the large vesicle growth. This supports the scaling cascading model for the coalescence of the large vesicles (Gaonac'h et al., 1996) which predicts $B \approx 1$ for large vesicles. Using the theoretical formula for sample vesicularity derived from this model and using the observed parameters, we find excellent agreement between the theoretical and empirical sample vesicularities. Furthermore, the theoretical vesicularity is the product of two terms; one sensitive to the largest vesicle present in the sample (it varies randomly), whereas the other (N^*A^*) depends on the volcanology/history. In particular, the product N^*A^* exhibits a systematic correlation with P_2, explaining the higher values of the initial 1985 source samples.

In recent years, the role of vesicles on lava morphology, rheology, and their associated emplacement styles has been increasingly recognized. The standard approach to the problem has been—in spite of the evident strong heterogeneity of the observed flows—to develop homogeneous models (e.g., of diffusion or growth by collision) and to characterize the vesicle distributions by single scales corresponding to median or other classical measures of characteristic size. In this paper, we have considered the heterogeneity as a fundamental aspect of the problem and developed statistical methods appropriate for handling strong variability over wide ranges of scale. The heterogeneous vesicularity leads to heterogeneous structure of a lava flow implying nonlinear dynamics. Hence, when collecting samples we have to keep in mind the large variability from one sample to another. More studies in this direction are necessary, particularly with more silicic magmas and lavas. These results also are expected to have implications for pumice (work in progress).

The discovery of new examples and types of volcanological scale invariance give more robustness to the general scaling approach to the volcanological phenomena. The scale invariance found for vesicles may be associated with the scale invariance of the lava morphology, and the outer scale "cut-offs" of the vesicle scaling may be the same (as the inner break of the scale invariance of the morphology). In the search for causes of the morphological scale invariance, we have beeen interested in one particular aspect of the rheology present at resolution of mm to meter scales in basaltic lavas. More work

must now be done to better constrain the inner limit of the scale invariance of the morphology and relate the different scale invariant sets or fields involved in the formation of lava flows.

Acknowledgements

We thank Dr. M. Pompilio for a sample and for his help in the field and Dr. R. Romano for his help in the chronology of the 1985 eruption. Thanks also for fruitful discussions with Dr. C. Kilburn. We thank Dr. D.L. Sahagian and an anonymous reviewer for their critical comments. This research was supported by the Natural Sciences and Engineering Research Council of Canada, the Fonds pour La Formation de Chercheurs et l'Aide à la Recherche (Québec), and the Université de Montréal.

Appendix A

Transformation from one-dimensional to two-dimensional scaling exponents

Consider a vesicle population in a dimension space d (i.e., volume when $d = 3$, or "D volume" for fractal subspaces) whose size is L^d, where L is the linear measure of the size. We are interested in comparing the number (or with appropriate normalizations, probability) distributions in various subspaces, especially areal or linear sections and will only consider the case of statistical isotropy (where all the subspaces of interest have the same statistical properties independent of direction) and statistical homogeneity (where all the subspaces of interest have the same statistical properties independent of spatial location). Although this allows each individual vesicle to have arbitrary (even fractal) shapes and orientations, there is no overall preferential direction (the more general case involving differential stratification and rotation can be handled with Generalized Scale Invariance, Schertzer and Lovejoy, 1985). Strictly speaking, the result will apply to a group of statistically equivalent samples or to a single sufficiently large sample. In practice, number distributions empirically established over finite subspaces will only approximate the ensemble distribution.

The argument we used is similar to that establishing fractal codimensions are independent of the subspace (dimension-invariant) over which observations are made (for discussion, see Schertzer and Lovejoy, 1989, 1991). Denote by $P_{(d)}$, the fraction of space occupied by vesicles with sizes greater than L^d (the vesicularity distribution):

$$P_{(d)}(L'^d > L^d) \tag{A.1a}$$

is the contribution to the total vesicularity P due to vesicles with sizes $> L^d$. This vesicularity will be equal to the probability that a point taken at random on either the space or the sub-space will be on a vesicle size L^d or greater. The basic property we use is that for randomly sampled subspaces, that this probability does not depend on the subspace and its dimension. For example, for $d = 3, 2, 1$, we obtain:

$$P_3(V' > V) = P_2(A' > A) = P_1(L' > L) \tag{A.1b}$$

with $V = L^3$ and $A = L^2$. We can now consider the fraction of space occupied by vesicles with sizes between L^d and $L^d + \mathrm{d}(L^d)$, which is obtained by taking the differential of Eq. (A.2):

$$\mathrm{d}P = L^d n_d(L^d)\,\mathrm{d}(L^d) \tag{A.1c}$$

where n_d, the d-dimensional number density, is the number of randomly chosen vesicle cross sections on the subspace having size between L^d and $L^d + \mathrm{d}(L^d)$. The fraction of space $\mathrm{d}P$ is the same when estimated over any subspace (e.g. area, length, etc.) of the full space. Hence Eq. (A.1a) provides a dimension-invariant way of quantifying the vesicularity that could be used directly displaying empirical results, particularly when comparing different analysis techniques. We now consider the special cases where n_d is a power law with exponent $-(B_{(d)} + 1)$ over various ranges. The vesicularity distribution, number distribution, and number density are all related by:

$$\frac{1}{V}\left|\frac{\mathrm{d}P}{\mathrm{d}V}\right| = \left|\frac{\mathrm{d}N}{\mathrm{d}V}\right| = n(V) \tag{A.2}$$

The absolute value signs take into account the possibility that N can be defined as $N(V' > V)$, hence

$dN/dV = -n(V)$, or as $N(V' < V)$, hence $dN/dV = n(V)$.

Using this assumption:

$$n_d(L^d) \propto (L^d)^{-B_{(d)}-1} \quad \text{(A.3)}$$

$d(L_d)$ can be expressed as:

$$d(L^d) \propto dL^{d-1}dL \quad \text{(A.4a)}$$

then, dP is proportional to:

$$L^{-d(B_{(d)}-1)-1} \quad \text{(A.4b)}$$

We conclude that $d(B_{(d)} - 1)$ is invariant, which shows how scaling probabilities/densities can easily be transformed from one space to another. An immediate consequence is the special role played by the exponent $B_d = 1$ (invariant under intersections) which is associated with scale invariant vesicle distributions.

In practice the following special cases are particularly important:

$$B_3 = \tfrac{2}{3}B_2 + \tfrac{1}{3} \quad \text{(A.5)}$$

$$B_1 = 2B_2 - 1 \quad \text{(A.6)}$$

Appendix B

Exponents of the number distributions

As is frequent in geophysics, we will assume that the number distribution functions, the vesicularity and the number densities of the vesicles follow power law functions and are related as in Eq. (A.2). Because of divergences at small or large volumes, we will distinguish five different cases, carefully taking into account the constraint that the total vesicularity is bounded between 0 and 1. For simplicity, we treat only the volume distribution (B_3 case), although the entire discussion holds equally well for the area distributions (B_2 case) in lava cross sections.

B.1. $B > 1$:

This case is quite straightforward; the distribution decays with large V sufficiently rapidly so that we may take (for simplicity, we drop here the subscript value for P and B):

$$P(V' > V) = P^*\left(\frac{V}{V^*}\right)^{1-B} \quad V \geq V^* \quad \text{(A.7a)}$$

$$N(V' > V) = N^*\left(\frac{V}{V^*}\right)^{-B} \quad V \geq V^* \quad \text{(A.7b)}$$

with:

$$N^* = \frac{P^*}{V^*}\frac{B-1}{B}$$

The cut-off V^* is a characteristic size of the scaling regime (necessary to stop the vesicularity divergence at small V), N^* is the total number per unit volume corresponding to V^*, and $0 < P^* < 1$. Although for a large enough range of scaling, the largest vesicle will provide a negligeable contribution to the total vesicularity; in practice if B is not much bigger than 1, there may be significant fluctuations from sample to sample.

B.2. $0 \leq B \leq 1$:

When $B < 1$, from Eq. (A.7a), the vesicularity diverges for large V. It is therefore no longer possible to consider a pure power law vesicularity distribution with a lower scaling cut-off; the finiteness of the total vesicularity restricts the power law behaviour to $V \leq V^*$. Although for $B < 1$ the vesicularity distribution is bounded above, for $B > 0$ the number distribution will diverge for small V (this is not serious since the large number of small vesicles will not contribute significantly to the vesicularity). This divergence explains the change in the direction of the inequalities in the relations below:

$$P(V' < V) = P^*\left(\frac{V}{V^*}\right)^{1-B} \quad V \leq V^* \quad \text{(A.8a)}$$

$$N(V' > V) = \frac{(1-B)}{B}\frac{P^*}{V^*}\left[\left(\frac{V}{V^*}\right)^{-B} - 1\right] \quad V \leq V^* \quad \text{(A.8b)}$$

We have not used the symbol N^* since the total number of vesicles per volume is infinite. Of course

in practice, the largest observed V may be much smaller than V^* and the approximation $N(V' > V) = [(1-B)/B](P^*/V^*)(V/V^*)^{-B}$ may be used.

Two cases have to be considered: (1) This could apply to the small vesicle regime since, empirically, it might be the case for $B_2 \approx -0.40$, hence $B_3 \approx 0.05$ for small vesicles in normalized distributions (Section 3.4). In this case, the upper cut-off V^* is observed and corresponds to a transition from one type of behaviour (e.g., a power law with $0 \leq B \leq 1$), to a power law with different B. This cut-off will fundamentally determine the total vesicularity in this regime (Section 3.5 gives the result for a given largest vesicle present in an empirical sample). (2) This distribution may be relevant since the refined analyses seem to indicate $B_2 \approx 0.80$ ($B_3 \approx 0.85$, Section 3.4). It may also be the empirically relevant for the large vesicle regime case for the Hawaiian spongy pahoehoe ($B_2 \approx -0.2$; $B_3 \approx 0.2$). However, we may expect a break in the distribution due to another physical processes limiting the total vesicularity to < 1.

B.3. $B = 0$:

The case $B = 0$ may be relevant since it corresponds to $B_3 = 0$ and hence to the empirically observed small vesicle regime in individual Etnean samples with $B_2 \approx -0.5$. This case is special because the number density $n(V) \approx V^{-1}$ yields logarithmic form N. We can simply define the vesicularity distribution:

$$P(V' < V) = V\frac{P^*}{V^*} \quad V \leq V^* \tag{A.9a}$$

and hence:

$$N(V' > V) = \frac{P^*}{V^*} \ln \frac{V^*}{V} \quad V \leq V^* \tag{A.9b}$$

Once again, the fact that the number distribution diverges for small vesicles [5] is unimportant since its contribution to the vesicularity is negligible. $n(V) \approx V^{-1}$ is equivalent to a uniform volume number density defined in classes of $\xi = \ln V$ [$n(V)\mathrm{d}V = n_\xi(\xi)\mathrm{d}\xi$; $n_\xi(\xi) = \text{constant}$].

B.4. $B < 0$:

Both the vesicularity and number distributions converge for small V, so that this case is straightforward, we have:

$$P(V' < V) = P^*\left(\frac{V}{V^*}\right)^{1-B} \quad V \leq V^* \tag{A.10a}$$

$$N(V' < V) = N^*\left(\frac{V}{V^*}\right)^{-B} \quad V \leq V^* \tag{A.10b}$$

with:

$$N^* = \frac{(B-1)}{B}\frac{P^*}{V^*}$$

It is interesting to note that by changing the dimension of space, we may change the sign of B. It is therefore possible (and empirically possibly relevant since $B_2 \approx -0.40$, $B_3 > 0$) that studying areal cross sections will lead to a finite number of small vesicles per unit area, whereas, studying the volumes would lead to an infinite number of vesicles per unit volume. The whole point is that the vesicularity distribution rather than the number distribution is physically significant, and this remains invariant. The large number of very small vesicles is simply irrelevant to the vesicularity. This underscores the dangers of judging the significance of different physical processes (e.g., diffusion vs. coalescence) by considering the relative number of vesicles involved.

B.5. The special case $B = 1$

The vesicle distribution will clearly be the result of complex non-linear lava dynamics. However, we have argued that—at least over certain scale ranges—the dynamics will have no characteristic scale, and will therefore respect scaling symmetries (i.e., some aspect, typically an exponent, will be invariant under scale changes). Up until now, we have made the automatic identification of scaling with power law distributions; this was adequate for our purposes. Unfortunately, this is not enough for the case $B = 1$,

[5] Actually, if necessary, in this marginal case, we may introduce logarithmic corrections to P which can allow for the small V convergence of the total number of vesicles per unit volume.

since a pure power law with this exponent will involve both small and large V divergences in the all-important vesicularity distribution.

Although power laws are the only distributions that exactly maintain their form for all V under a "zoom" (scale change) ratio λ (i.e., under the transformation $V \rightarrow \lambda^3 V$), we have already seen that an inner or outer cut-off is necessary if such distributions are to provide useful models for vesicle sizes. More generally, functions of the form:

$$V^{1-B}(\ln V)^{1-s}(\ln\ln V)^{1-t}\ldots$$

will also maintain their forms under "zooms"—at least for large (or small) enough V. The new scaling exponents s, t, etc. can be considered second, third and higher order corrections to the basic scaling V^{1-B}. When $B \neq 1$, these corrections will be small and very difficult (if not impossible) to empirically detect (or theoretically model), and we have ignored them. However, clearly when $B = 1$, the logarithmic correction $(\ln V)^{1-s}$ becomes first order (dominant) and must be considered. In this case (ignoring third and higher order corrections) we may take the following vesicularity distribution:

$$P(V' > V) = P^*\left(1 + \ln\frac{V}{V^*}\right)^{1-s} \quad V \geq V^* \tag{A.11a}$$

with $s > 1$ (we will not consider $s < 1$ which involves an upper rather than lower cut-off, nor $s = 1$ which involves "ln ln corrections").

To within smaller order terms (i.e., to within a term of order $1 + \ln(V/V^*)^{-s-1}$, this corresponds to the following number distribution:

$$N(V' > V) \approx N^*\left(\frac{V}{V^*}\right)^{-1}\left(1 + \ln\frac{V}{V^*}\right)^{-s} \quad V \geq V^* \tag{A.12a}$$

Due to the slow variation in the logarithmic term, this yields the approximation:

$$N(V' > V) \approx N^*\frac{V^*}{V} \quad V \geq V^* \tag{A.12b}$$

We introduced the "ln corrections" in order to be able to maintain scaling distributions with only a single cut-off. If we are willing to introduce both a lower and an upper cut-off, the mathematical treatment is a bit simpler, but the implications for the vesicularity will be the same.

References

Aubele, J.C., Crumpler, L.S. and Elston, W.E., 1988. Vesicle zonation and vertical structure of basalt flows. J. Volcanol. Geotherm. Res., 35: 349–374.

Bagdassarov, N.S. and Dingwell, D.B., 1993. Deformation of foamed rhyolites under internal and external stresses: an experimental investigation. Bull. Volcanol., 55: 147–154.

Bak, P., Tang, C. and Weiessenfeld, K., 1987. Self-Organized Criticality: An explanation of $1/f$ noise. Phys. Rev. Lett., 59: 381–384.

Barbieri, F., Carapezza, M.L., Valenza, M. and Villari, L., 1993. The control of lava flow during the 1991–1992 eruption of Mt. Etna. J. Volcanol. Geotherm. Res., 56: 1–34.

Blackburn, E.A., Wilson, L. and Sparks, R.S.J., 1976. Mechanisms and dynamics of Strombolian activity. J. Geol. Soc. London, 132: 429–440.

Bruno, B.C., Taylor, G.J., Rowland, S.K., Lucey, P.G. and Self, S., 1992. Lava flows are fractals. Geophys. Res. Lett., 19: 305–308.

Carbone, D.A.M., 1993. Analisi tessiturale quantitativa di una sezione di flusso lavico dell'eruzione etnea 1991–1993. Thesis, Univ. Catania.

Cashman, K.V., Mangan, M.T. and Newman, S., 1994. Surface degassing and modifications to vesicle size distributions in active basalt flows. J. Volcanol. Geotherm. Res., 61: 45–68.

Chester, D.K., Duncan, A.M., Guest, J.E. and Kilburn, C.R.J., 1985. Mount Etna: the Anatomy of a Volcano. Chapman and Hall, London.

Dubois, J. and Cheminée, J.L., 1991. Fractal analysis of eruptive activity of some basaltic volcanoes. J. Volcanol. Geotherm. Res., 45: 197–208.

Falconer, K., 1990. Fractal Geometry, Mathematical Foundations and Applications. Wiley, 288 pp.

Gaonac'h, H., 1994. L'hétérogénéité de la morphologie et de la rhéologie des laves: scaling et fractales. Thèse Ph.D., Univ. Montréal.

Gaonac'h, H., Lovejoy, S. and Stix, J., 1992. Scale invariance of basaltic lava flows and their fractal dimensions. Geophys. Res. Lett., 19: 785–788.

Gaonac'h, H., Lovejoy, S., Stix, J. and Schertzer, D., 1996. A scaling growth model for bubbles in basaltic lava flows. Earth Planet. Sci. Lett., 139: 395–409.

Gutenberg, R., 1944. Frequency of earthquakes in California. Bull. Seismol. Soc. Am., 34: 185–188.

Jaupart, C., 1991. Effects of compressibility on the flow of lava. Bull. Volcanol., 54: 109.

Jaupart, C. and Vergniolle, S., 1988. Laboratory models of Hawaiian and Strombolian eruptions. Nature, 331: 58–60.

Keszthelyi, L., 1994. Calculated effect of vesicles on the thermal properties of cooling basaltic lava flows. J. Volcanol. Geotherm. Res., 63: 257–266.

Korchak, J., 1938. Deux types fondamentaux de distribution statistique. Bull. Inst. Stat., III: 295–299.

Lavallée, D., Lovejoy, S., Schertzer, D. and Ladoy, P., 1993. Nonlinear variability of landscape topography: multifractal analysis and simulation. In: L. Decola and N. Lam (Editors), Fractals in Geography. Prentice-Hall, Englewood Cliffs, NJ, pp. 158–192.

Mandelbrot, B., 1983. The Fractal Geometry of Nature. Freeman, San Francisco, CA.

Mangan, M.T., Cashman, K.V. and Newman, S., 1993. Vesiculation of basaltic magma during eruption. Geology, 21: 157–160.

McMillan, K., Long, P.E. and Cross, R.W., 1989. Vesiculation in Columbia River basalts. Geol. Soc. Am., 239: 157–167.

Sahagian, D.L., 1985. Bubble migration and coalescence during the solidification of basaltic lava flows. J. Geol., 93: 205–211.

Sahagian, D.L., Anderson, A.T. and Ward, B., 1989. Bubble coalescence in basalt flows: comparison of a numerical model with natural examples. Bull. Volcanol., 52: 49–56.

Sarda, P. and Graham, D., 1990. Mid-ocean ridge popping rocks: implications for degassing at ridge crests. Earth Planet. Sci. Lett., 97: 268–289.

Schertzer, D. and Lovejoy, S., 1985. Generalised scale invariance in turbulent phenomena. Phys. Chem. Hydrol. J., 6: 623–635.

Schertzer, D. and Lovejoy, S., 1987. Physically based rain and cloud modeling by anisotropic, multiplicative turbulent cascades. J. Geophys. Res., 92: 9692–9714.

Schertzer, D. and Lovejoy, S., 1989. Nonlinear variability in geophysics: multifractal analysis and simulations. In: L. Pietronero (Editor), Fractals, Their Physical Origins and Properties. Plenum Press, New York, NY, pp. 49–79.

Schertzer, D. and Lovejoy, S., 1991. Nonlinear Variability in Geophysics: Scaling and Fractals. Kluwer, Dordrecht.

Schertzer, D. and Lovejoy, S., 1994. Multifractal generation of self-organized criticality. In: M. Novak (Editor), Fractals in the Natural and Applied Sciences. Elsevier, Amsterdam, pp. 325–339.

Schertzer, D. and Lovejoy, S., 1996. The multifractal phase transition route to self-organized criticality in turbulence and other dissipative nonlinear systems. Phys. Rep. (in press).

Sornette, A., Dubois, J., Cheminée, J.L. and Sornette, D., 1991. Are sequences of volcanic eruptions deterministically chaotic? J. Geophys. Res., 96: 11,931–11,945.

Sparks, R.S.J., 1978. The dynamic of bubble formation and growth in magmas: a review and analysis. J. Volcanol. Geotherm. Res., 3: 1–37.

Stein, D.J. and Spera, F.J., 1992. Rheology and microstructure of magmatic emulsions: theory and experiments. J. Volcanol. Geotherm. Res., 49: 157–174.

Toramaru, A., 1990. Measurement of bubble size distributions in vesiculated rocks with the implications for quantitative estimation of eruption processes. J. Volcanol. Geotherm. Res., 43: 71–90.

Vergniolle, S. and Jaupart, C., 1986. Separated two-phase flow and basaltic eruptions. J. Geophys. Res., 91: 12,842–12,860.

Walker, G.P.L., 1989. Spongy pahoehoe in Hawaii: a study of vesicle-distribution patterns in basalt and their significance. Bull. Volcanol., 51: 199–209.

Wilmoth, R.A. and Walker, G.P.L., 1993. P-type and S-type pahoehoe: a study of vesicle distribution patterns n Hawaiian lava flows. J. Volcanol. Geotherm. Res., 55: 129–142.